

# Experiments and Modeling of the Autoignition of Methyl ~~Valerate~~ Pentanoate at Low to Intermediate Temperatures and Elevated Pressures in a Rapid Compression Machine

Bryan W. Weber<sup>a,\*</sup>, Justin A. Bunnell<sup>a</sup>, Kamal Kumar<sup>b</sup>, Chih-Jen Sung<sup>a</sup>

<sup>a</sup>*Department of Mechanical Engineering, University of Connecticut, Storrs, CT, USA*

<sup>b</sup>*Department of Mechanical Engineering, University of Idaho, Moscow, ID, USA*

---

## Abstract

Methyl valerate ( $\text{C}_6\text{H}_{12}\text{O}_2$ , methyl pentanoate) is a methyl ester and a relevant surrogate component for biodiesel. In this work, we present ignition delays of methyl valerate measured using a rapid compression machine at a range of engine-relevant temperature, pressure, and equivalence ratio conditions. The conditions we have studied include equivalence ratios ( $\phi$ ) from 0.25 to 2.0, temperatures between 680 K and 1050 K, and pressures of 15 bar and 30 bar. The ignition delay data demonstrate a negative temperature coefficient region in the temperature range of 720 K–800 K for both  $\phi = 2.0$ , 15 bar and  $\phi = 1.0$ , 30 bar, with two-stage ignition apparent over the narrower temperature ranges of 720 K–760 K for 15 bar and 740 K–760 K at 30 bar. In addition, the experimental ignition delay data are compared with simulations using an existing chemical kinetic model from the literature. The simulations with the literature model under-predict the data by factors between 2 and 10 over the entire range of the experimental data. In addition, a new chemical kinetic model is developed using the Reaction Mechanism Generator (RMG) software. The agreement between the experimental data and the RMG model is also not satisfactory. To help determine the possible reasons for the disagreement, a path analysis of both models is completed. It is found that improvements to both the reaction

---

\*Corresponding Author: bryan.weber@uconn.edu

pathways and thermodynamic properties are required. Further directions for future improvement of the methyl valerate model are discussed.

*Keywords:* chemical kinetics, rapid compression machine, autoignition, methyl ester, methyl valerate, methyl pentanoate

---

## 1. Introduction

For transportation applications, biodiesel is an important constituent in improving environmental friendliness of fuels. This is due to its renewability when produced from sustainable agricultural crops and its ability to reduce emissions relative to petroleum-derived fuels [1]. Biodiesel typically consists of long-chain methyl ester molecules, with typical compositions of  $C_{14}$  to  $C_{20}$  [1]. Recognizing that the large molecular size of the methyl esters within biodiesel fuel makes creating and using detailed chemical kinetic models challenging [2], it is desired to study their combustion chemistry by studying simpler methyl ester molecules.

A recent review paper summarizes the work on methyl esters relevant to biodiesel combustion [3]; the following summary focuses on ignition delay measurements, since these are the focus of this paper. Autoignition of methyl butanoate (MB,  $C_5H_{10}O_2$ ) has been well-studied in both shock tube and rapid compression machine experiments [4–10]. The prevalence of MB data in the literature is largely due to the early identification of MB as a potential surrogate fuel for biodiesel [11]. However, the [literature](#) experiments have shown that MB may not be an appropriate surrogate for biodiesel, due to its lack of negative temperature coefficient (NTC) behavior, a requirement for a suitable biodiesel surrogate [3].

Methyl esters larger than MB, such as methyl valerate (MV,  $C_6H_{12}O_2$ , methyl pentanoate), have also been studied as possible biodiesel surrogates. Hadj-Ali et al. [9] used a rapid compression machine (RCM) to study the autoignition of several methyl esters including MV. Although MV exhibited two-stage ignition in this study, little additional research has been done on its low-

26 temperature chemistry. Korobeinichev et al. [12] studied MV in premixed lam-  
 27 inar flames and extended a detailed high temperature chemical kinetic model  
 28 to include MV and methyl hexanoate. Dmitriev et al. [13] added MV to n-  
 29 heptane/toluene fuel blends to determine the resulting intermediate species in  
 30 premixed flames using a flat burner at 1 atm and an equivalence ratio of 1.75.  
 31 The addition of MV helped reduce soot forming intermediates including ben-  
 32 zene, cyclopentadienyl, acetylene, propargyl, and vinylacetylene [13]. Hayes  
 33 and Burgess [14] computationally examined the peroxy radical isomerization  
 34 reactions for MV to better understand the low temperature reaction pathways.  
 35 Finally, Diévert et al. [15] used diffusion flames in the counterflow configuration  
 36 to determine extinction limits for a number of methyl esters, including MV, and  
 37 validated a detailed kinetic model with the experimental data.

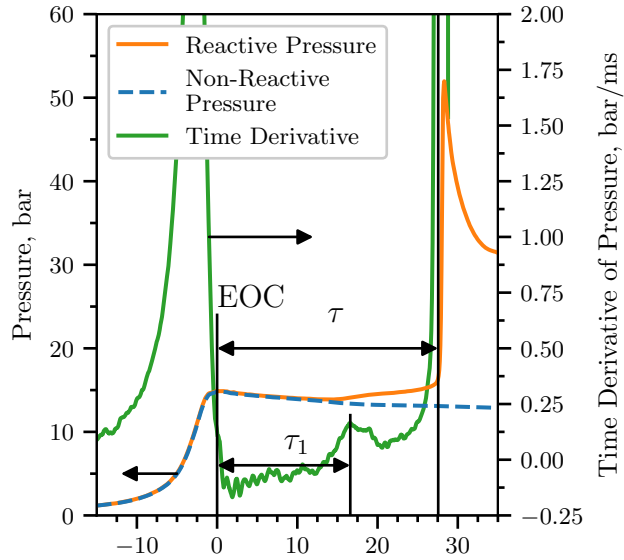
38 This work provides additional data for the autoignition of MV. Data is col-  
 39 lected in a RCM under engine relevant conditions spanning from 15 bar to 30 bar,  
 40 equivalence ratios ( $\phi$ ) from 0.25 to 2.0, and temperatures from 680 K to 1050 K.  
 41 The NTC region of MV is mapped out to provide additional information on the  
 42 fidelity of using MV as a biodiesel surrogate [and insights into the autoignition](#)  
 43 [chemistry of large methyl esters](#).

## 44 2. Experimental Methods

45 The RCM used in this study is a single piston arrangement and is pneu-  
 46 matically driven and hydraulically stopped. The device has been described in  
 47 detail previously [16] and will be described here briefly for reference. The end  
 48 of compression (EOC) temperature and pressure ( $T_C$  and  $P_C$  respectively), are  
 49 independently changed by varying the overall compression ratio, initial pressure  
 50 ( $P_0$ ), initial temperature ( $T_0$ ), and specific heat ratio of the experiments. The  
 51 piston in the reaction chamber is machined with a specially designed crevice to  
 52 suppress the roll-up vortex effect and promote homogeneous conditions in the  
 53 reactor during and after compression [17].

54 The primary diagnostic on the RCM is the in-cylinder pressure measured by

55 a Kistler 6125C dynamic transducer that is compensated for thermal shock. The  
 56 transducer is coupled to a Kistler 5010B charge amplifier. The voltage output  
 57 of the charge amplifier is recorded by a National Instruments 9125 analog input  
 58 device connected to a cDAQ 9178 chassis. The voltage is sampled at a rate of  
 59 either 50 kHz or 100 kHz by a LabView VI and processed by a Python package  
 60 called UConnRCMPy [18]. Version 3.0.5 of UConnRCMPy [19], 3.6 of Python,  
 61 2.3.0 of Cantera [20], 1.13.0 of NumPy [21], 0.19.0 of SciPy [22], and 2.0.1 of  
 62 Matplotlib [23] are used in the analysis in this paper.



63

Figure 1: Definition of the ignition delays used in this work. The experiment in this figure is  
 conducted for a  $\phi = 2.0$  mixture with  $\text{Ar}/(\text{N}_2 + \text{Ar}) = 0.5$ ,  $P_0 = 0.7806$  bar,  $T_0 = 373$  K,  $P_C =$   
 14.92 bar,  $T_C = 720$  K,  $\tau = (27.56 \pm 0.89)$  ms, and  $\tau_1 = (16.60 \pm 0.46)$  ms. [The non-reacting](#)  
 64 [pressure trace by replacing  \$\text{O}\_2\$  with  \$\text{N}\_2\$  is also shown for reference.](#)

65 The compression stroke of the RCM brings the fuel/oxidizer mixture to the  
 66 EOC conditions, and for suitable thermodynamic states, the mixture will ignite  
 67 after a delay period. The definitions of the ignition delays are shown in Fig. 1.  
 68 The time of the EOC is defined as the maximum of the pressure trace prior to  
 69 the start of ignition and the ignition delays are defined as the time from the EOC

until local maxima in the first time derivative of the pressure. Each experimental condition is repeated at least five times to ensure repeatability of the data. As there is some random scatter present in the data, the standard deviation ( $\sigma$ ) of the ignition delays from the runs at a given condition is computed. Typically,  $\sigma$  is less than 10 % of the mean values of the overall ignition delay ( $\tau$ ) and the first stage ignition delay ( $\tau_1$ ).

In addition to the reactive experiments, non-reactive experiments are conducted by replacing  $O_2$  with  $N_2$  to determine the influence of machine-specific behavior on the experimental conditions (see Fig. 1) and permit the calculation of the EOC temperature via the isentropic relations between pressure and temperature [24]. The EOC temperature is calculated by the procedure described in Section 3.

The mixtures considered in this study are shown in Table 1. Four equivalence ratios of MV in “air” are considered. While  $O_2$  is kept at 21 % by mole in the oxidizer, the ratio of Ar :  $N_2$  in the oxidizer is varied to adjust the temperatures reached at the EOC. Two  $P_C$  conditions are studied in this work, 15 bar and 30 bar, representing engine-relevant conditions. For the  $\phi = 2.0$  condition, only  $P_C = 15$  bar is considered because we could not achieve  $T_C$  values low enough that the ignition during the compression stroke can be prevented.

Table 1: Mixtures considered in this work

$\phi$	Mole Fraction (purity)				Ar/( $N_2 + Ar$ )
	MV (100 %)	$O_2$ (99.994 %)	Ar (99.999 %)	$N_2$ (99.999 %)	
0.25	0.0065	0.2087	0.7848	0.0000	1.0
0.5	0.0130	0.2074	0.7796	0.0000	1.0
1.0	0.0256	0.2047	0.7697	0.0000	1.0
1.0	0.0256	0.2047	0.3849	0.3848	0.5
2.0	0.0499	0.1996	0.0000	0.7505	0.0
2.0	0.0499	0.1996	0.3752	0.3753	0.5

Mixtures are prepared in stainless steel mixing tanks, 17 L and 15 L in size. The proportions of reactants in the mixture are determined by specifying the absolute mass of the fuel, the equivalence ratio, and the ratio of Ar : N<sub>2</sub> in the oxidizer. Mixtures are made by first vacuuming the mixing tanks to an ultimate pressure less than 5 Torr. Since MV is a liquid with a relatively small vapor pressure at room temperature and pressure, it is measured gravimetrically to within 0.01 g of the specified value. The fuel is injected into the mixing tank through a septum. Proportions of O<sub>2</sub>, Ar, and N<sub>2</sub> are added manometrically at room temperature and the total pressure is measured by an Omega Engineering MMA100V10T2D0T4A6 type static pressure transducer. The same transducer is used to measure the pressure of the ~~reactants~~ reactant mixture prior to an experiment.

The RCM is equipped with heaters to control the initial temperature of the mixture. After filling in the components to the mixing tanks, the heaters are switched on and the system is allowed 1.5 h to come to steady state. The mixing tanks are also equipped with magnetic stir bars so the reactants are well mixed for the duration of the experiments. Previous work has shown this procedure to completely vaporize the fuel and prevent fuel cracking during the heating process [25–27].

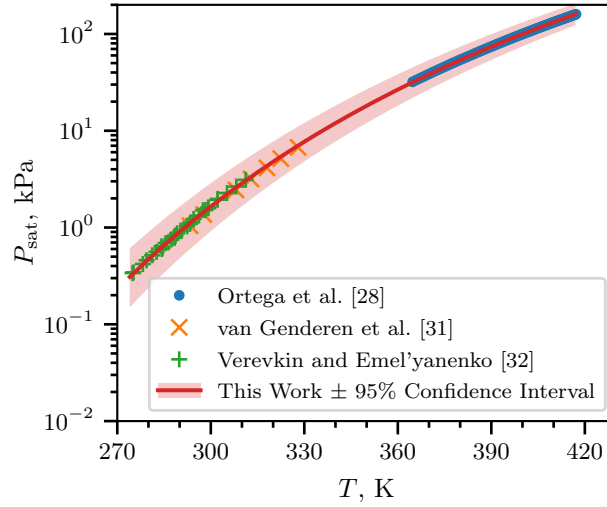
~~Saturated vapor pressure of MV as a function of temperature, plotted using the Antoine equation, Eq. (1), with  $A = 6.4030$ ,  $B = 1528.69$ , and  $C = 52.881$ .~~

The initial temperature is chosen such that the saturated vapor pressure ( $P_{\text{sat}}$ ) of the fuel at the initial temperature is at least twice the partial pressure of the fuel in the mixing tank. The Antoine equation

$$\log_{10} P_{\text{sat}} = A - \frac{B}{T - C} \quad (1)$$

is used to model the saturated vapor pressure of MV as a function of temperature ( $T$ ), where  $A$ ,  $B$ , and  $C$  are substance-specific coefficients, given in units of K and kPa. Coefficients for Eq. (1) are given in the literature by Ortega et al. [28], Camacho et al. [29], and Stephenson et al. [30]. Unfortunately, the values of the coefficients are different among all three references. Therefore, coefficients for

119 use in Eq. (1) are determined in this work by least squares fitting of the data  
 120 of Ortega et al. [28], van Genderen et al. [31], and Verevkin and Emel'yanenko  
 121 [32] using the `curve_fit()` function of SciPy [22] version 0.19.0. Figure 2  
 122 shows that the coefficients fitted with this procedure give good agreement with  
 123 the experimental data; values for the coefficients computed in this work and  
 124 [reported](#) in the literature works are given in Table 2. The data and code used  
 125 to calculate the coefficients are provided in the Supplementary Material.



126

Figure 2: [Saturated vapor pressure of MV as a function of temperature, plotted using the Antoine equation, Eq. \(1\), with  \$A = 6.4030\$ ,  \$B = 1528.69\$ , and  \$C = 52.881\$ .](#)

Table 2: Antoine Equation coefficients computed in this work and [obtained](#) from the literature, [in units of K and kPa](#). The  $2\sigma$  confidence interval is estimated by taking the square root of the diagonals of the covariance matrix returned from `curve_fit()`

	$A$	$B$	$C$	$T_{\min}$ , K	$T_{\max}$ , K
This Work	6.4030	1528.69	52.881	274.9	417.18
2 $\sigma$ Confidence Interval	0.0919	53.47	4.934	—	—
Ortega et al. [28]	6.23175	1429.00	62.30	364.75	417.18
Camacho et al. [29]	5.9644	1281.06	75.94	281	547
Stephenson et al. [30]	6.62646	1658.4	42.09	297	411

### 3. Computational Methods

#### 3.1. RCM Modeling

The Python 3.6 interface of Cantera [20] version 2.3.0 is used for all simulations in this work. Detailed descriptions of the use of Cantera for these simulations can be found in the work of Weber and Sung [18] and Dames et al. [33]; a brief overview is given here. As mentioned in Section 2, non-reactive experiments are conducted to characterize the machine-specific effects on the experimental conditions in the RCM. This pressure trace is combined with the reactive pressure trace and used to compute a volume trace by assuming that the reactants undergo a reversible, adiabatic, constant composition (i.e., isentropic) compression during the compression stroke and an isentropic expansion after the EOC. The volume trace is applied to a simulation conducted in an `IdealGasReactor` in Cantera [20] using the CVODES solver from the SUNDIALS suite [34]. The ignition delays from the simulations are defined in the same manner as in the experiments. The time derivative of the pressure in the simulation is computed by second order Lagrange polynomials, as discussed by Chapra and Canale [35]. The volume trace files, the corresponding pressure traces, and `volume-trace.yaml` files suitable for use with UConnRCMPy v3.0.5 [19] are available on the web at <https://combdialab.engr.uconn.edu/database/rcm-database> and on figshare at <https://doi.org/10.6084/m9.figshare.5213341>. In addition, ChemKED-format [36] files are available in the main ChemKED database repository at <https://github.com/pr-ometh-us/ChemKED-database>.



153 To the best of our knowledge, there are three mechanisms for MV com-  
 154 bustion available in the literature. The first two, by Korobeinichev et al. [12]  
 155 and Dmitriev et al. [13], were developed to simulate flames, and do not include  
 156 the low-temperature chemistry necessary to simulate the conditions in ~~these the~~  
 157 current RCM experiments. The third model was developed by Diévaré et al. [15]  
 158 and includes low-temperature chemistry of MV, although it was only validated  
 159 by comparison with flame extinction limits. In converting this mechanism for  
 160 use in Cantera, we found that there were many species in the thermodynamic  
 161 database with multiple data entries. For most of these species the thermody-  
 162 namic data is identical. However, some species are not exact duplicates. For  
 163 these species, it is not clear from the thermodynamic database file which data set  
 164 should be preferred. Since Cantera (and CHEMKIN) choose the first instance  
 165 of a duplicate species to be used, we retained the first entry for all duplicated  
 166 species. The detailed model of Diévaré et al. [15] includes 1105 species and 7141  
 167 reactions, and the Cantera formatted input file is available in the Supplementary  
 168 Material.

### 169 3.2. Reaction Mechanism Generator

170 In addition to using a mechanism from the literature, we investigate the  
 171 use of an automatic mechanism generator, the open-source Reaction Mecha-  
 172 nism Generator (RMG) [37] version 2.1.0. The Python version of RMG is used,  
 173 which requires Python 2.7, and version 2.1.0 of the RMG database is used.  
 174 The final RMG model contains 427 species and 13640 reactions. Note that the  
 175 number of species is much lower than the Diévaré et al. [15] model because the  
 176 RMG model focuses on only one fuel (MV), but the number of reactions is sub-  
 177 stantially higher. The input file used to generate the model is available in the  
 178 Supplementary Material. In addition, the CHEMKIN and Cantera formatted  
 179 input files for the ~~RMG~~ RMG-generated model are available in the Supplemen-  
 180 tary Material.

## 181 4. Experimental Results

### 182 4.1. Ignition Delays

183 Figure 3 shows the ignition delay results measured in this study. Filled mark-  
184 ers denote the overall ignition delay and hollow markers indicate the first-stage  
185 ignition delay. Vertical error bars are drawn on the symbols to represent the  $2\sigma$   
186 uncertainty in the ignition delay; for many of the experiments, the uncertainty  
187 is approximately the same size as the data point, so the error bar is hidden.  
188 Horizontal error bars are shown on the first and last points of each equivalence  
189 ratio indicating the estimated uncertainty in the EOC temperature of  $\pm 1\%$  [38].  
190 Fig. 3a shows the results for a compressed pressure of 15 bar, while Fig. 3b shows  
191 the results for a compressed pressure of 30 bar. Note that  $\phi = 2.0$  results were  
192 not collected for 30 bar, so there are no red triangle data points in Fig. 3b. A  
193 summary of the ignition delay data is available as a comma-separated value  
194 file in the Supplementary Material, [including the mixture conditions for each](#)  
195 [experiment, the initial conditions, the compressed conditions, and the ignition](#)  
196 [delays and their associated errors.](#)

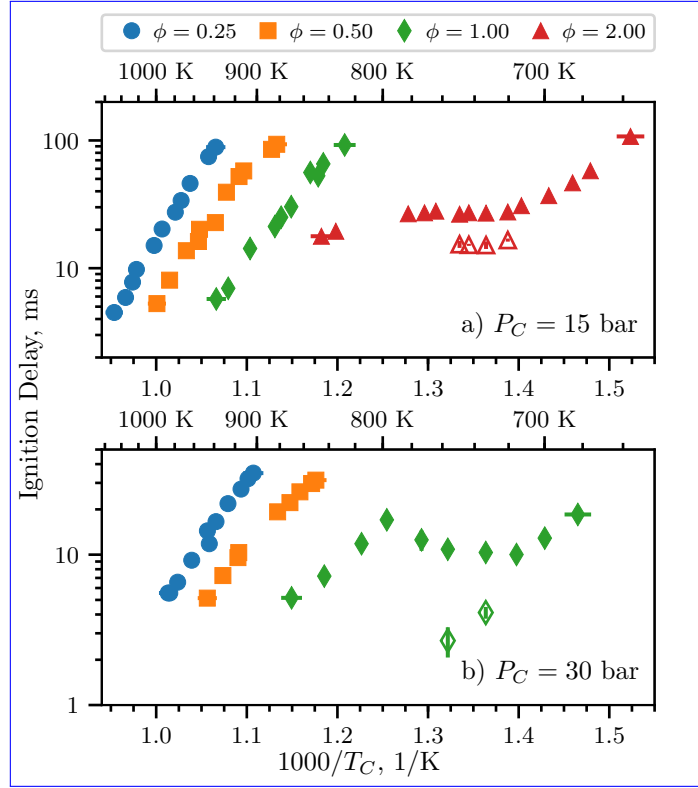


Figure 3: Ignition delays of MV as a function of inverse temperature for varying equivalence ratios. Filled points are the overall ignition delays and hollow points are the first stage ignition delays. a) 15 bar, b) 30 bar.

It can be seen from Fig. 3 that the ignition delays for the  $\phi = 0.25$  and 0.5 mixtures do not show an NTC region of the ignition delay for both of the pressures studied in this work. However, the  $\phi = 1.0$  mixture shows an NTC region at  $P_C = 30$  bar between approximately 720 K and 800 K, with measured first-stage ignition delays at 733 K and 757 K. In addition, the  $\phi = 2.0$  mixture shows an NTC region of ignition delay at 15 bar from approximately 720 K to 780 K, with measured first-stage ignition delays between 720 K and 750 K.

~~Ignition delays of MV as a function of inverse temperature for varying equivalence ratios. Filled points are the overall ignition delays and hollow points are the first stage ignition delays. a) 15 bar, b) 30 bar.~~

Hadj-Ali et al. [9] also observed two-stage ignition of MV in stoichiometric

210 mixtures, stating that “[m]ethyl pentanoate... was more reactive [than methyl  
 211 butanoate] with a limit below which autoignition no longer occurs observed at  
 212  $T_c = 670$  K and  $P_c = 11.4$  bar. At this temperature, the autoignition occurred  
 213 in two stages with a clearly identified cool flame event.” However, we do not  
 214 find ~~two-stage~~ two-stage ignition for the similar pressure of  $P_C = 15$  bar in  
 215 this study. We note that the stated temperature of the experiment from the  
 216 work of Hadj-Ali et al. [9] (670 K) is much lower than the lowest temperature  
 217 we considered in this work at 15 bar,  $\phi = 1.0$  (828 K). We did not conduct  
 218 experiments at lower temperatures because the work of Mittal and Sung [17]  
 219 showed that the temperature field in the RCM reaction chamber was uniform  
 220 for approximately 100 ms after the EOC, and our measured ignition delay at  
 221 15 bar,  $\phi = 1.0$ , and 828 K is 92.14 ms.

222 However, we ~~note~~ find NTC behavior of the overall ignition delay and two-  
 223 stage ignition at the higher pressure of 30 bar, and at higher temperatures than  
 224 those reported for two-stage ignition in the study of Hadj-Ali et al. [9]. The  
 225 trend of NTC behavior shifting to higher temperatures with increasing pressure  
 226 can be seen in other classes of fuels. Kukkadapu et al. [39] found a similar  
 227 trend in gasoline composed of iso-alkanes, n-alkanes, cyclo-alkanes, aromatics,  
 228 and olefins. Kukkadapu et al. [39] attributed the shift of the NTC region to the  
 229 reactions between the hydroperoxyalkyl radical (QOOH) and  $O_2$  becoming more  
 230 dominant than the unimolecular decomposition of QOOH at higher pressures.  
 231 Similar trends could occur for the hydroperoxyalkyl radicals of MV.

232 To further understand the effect of the methyl ester functional group on the  
 233 NTC region of ignition delay, we compare with the alkane and alcohol with  
 234 5-carbon alkyl chains, n-pentane and n-pentanol. n-Pentane and MV have the  
 235 same fuel mole percentage for stoichiometric mixtures in air (2.56 %), while  
 236 n-pentanol has a fuel mole percentage of 2.72 % for stoichiometric conditions.  
 237 Ribaucour et al. [40] and Bugler et al. [41] found the NTC region for n-pentane  
 238 to be between 760 K and 910 K at pressures near 10 atm. As we will compare  
 239 with our MV data at 30 bar, we note that increasing the pressure tends to shift  
 240 the NTC to higher temperatures, as mentioned previously [39]. Heufer et al. [42]

found NTC behavior for n-pentanol in the range of 770 K to 900 K at 30 bar. In this study, we find the NTC window for MV at 30 bar to be between 720 K and 800 K. Therefore, it appears that the methyl ester functional group causes the NTC range to occur at lower temperature as compared to alkanes and alcohols with similar alkyl chain lengths. This result was also noted by Hadj-Ali et al. [9] for methyl hexanoate as the fuel.

#### 4.2. Pressure Traces

Figure 4a shows the pressure traces for selected experiments at  $\phi = 1.0$ ,  $P_C = 30$  bar. The three reactive pressure traces shown are at the low-temperature end of the NTC (blue, 700 K), one case with two-stage ignition (orange, 733 K), and one case near the high-temperature limit of the NTC region (green, 774 K). Also shown is the non-reactive pressure trace for the 700 K case (red). By comparing the 700 K pressure trace with the non-reactive pressure trace, it can be seen that there is substantial heat release prior to main ignition as measured by the deviation of the reactive pressure trace from the non-reactive trace. However, there is only one peak in the time derivative of the pressure, so no first-stage ignition delay is defined for this case. It can also be seen in Fig. 4a that the 774 K case shows some heat release prior to ignition, although again there is only one peak in the time derivative of the pressure. Furthermore, the heat release at 774 K appears to be more gradual than at 700 K.

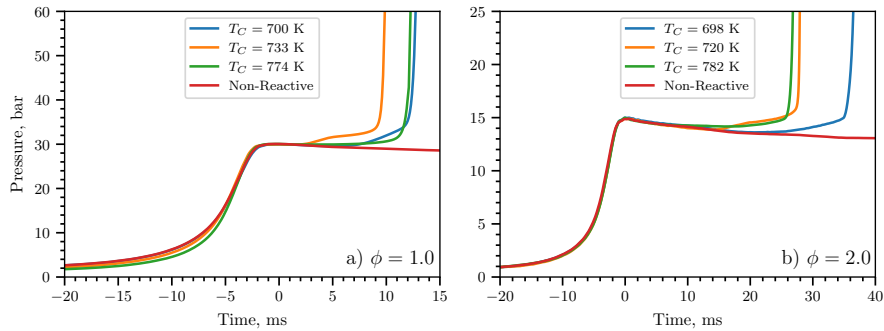


Figure 4: Selected pressure traces around the NTC region of ignition delay. a)

~~$\phi = 1.0, P_C = 30 \text{ bar}$~~   $\phi = 1.0, P_C = 30 \text{ bar}$ , b)  ~~$\phi = 2.0, P_C = 15 \text{ bar}$~~   $\phi = 2.0, P_C = 15 \text{ bar}$ .

The corresponding non-reactive pressure traces are also included for reference.

A similar trend can be observed in Fig. 4b for  $\phi = 2.0$  at  $P_C = 15 \text{ bar}$ , where pressure traces at several points around the NTC region are plotted. As in Fig. 4a, the three reactive pressure traces shown are at the low-temperature end of the NTC (blue, 698 K), one case with two-stage ignition (orange, 720 K), and one case near the high-temperature limit of the NTC region (green, 782 K). Also shown is the non-reactive pressure trace for the 698 K case (red). As for the  $\phi = 1.0$  case, the pressure traces show significant heat release prior to the overall ignition, as judged by deviation from the non-reactive case.

## 5. Computational Results

Figure 5 compares experimentally measured overall ignition delays with ignition delays computed with the detailed model of Diévar et al. [15] (solid lines). Figure 5a shows results at  $P_C = 15 \text{ bar}$ , while Fig. 5b shows results at  $P_C = 30 \text{ bar}$ . Only some equivalence ratios are shown for each pressure condition; data and simulated results are not shown for cases where the reactive simulated temperature at the EOC deviated substantially from the non-reactive temperature due to heat release during the compression stroke. Furthermore, it is important to note that the model of Diévar et al. [15] was not validated for MV ignition delays, only for extinction strain rates.

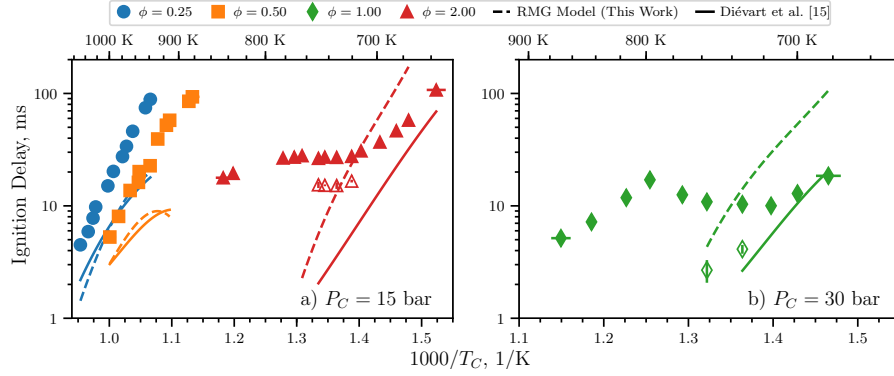


Figure 5: Comparison of experimental  $(\tau)$  and simulated  $(\tau)$  ignition delays computed using the procedure described in Section 3.1. a) 15 bar, b) 30 bar.

At 15 bar, the experimental overall ignition delays are under-predicted by the Diévert et al. [15] model for the three equivalence ratios shown. For the  $\phi = 0.25$  and 0.5 conditions, the model appears to be predicting an NTC region of the overall ignition delays as the temperature decreases, as judged by the increasing curvature of the simulations, although such a trend is not observed in the for the experimental data. However, at  $\phi = 2.0$ , the model does not predict the presence of an NTC region, although one is present in the experiments. Nonetheless, the agreement seems to be improving as the temperature is decreased. Comparing the Diévert et al. [15] model to the stoichiometric data at 30 bar, we find a similar trend as the  $\phi = 2.0$ ,  $P_C = 15$  bar  $\phi = 2.0$ ,  $P_C = 15$  bar data. The model does not predict the NTC region found experimentally for the  $\phi = 1.0$ ,  $P_C = 30$  bar experiments, but the agreement improves as the temperature decreases. Interestingly, two-stage ignition is predicted for all of the  $\phi = 1.0$  and  $\phi = 2.0$  data shown in Fig. 5. However, the first-stage ignition delays are 0.1 ms to 0.5 ms less than the overall ignition delays, and are not shown on Fig. 5 because they are nearly indistinguishable from the overall ignition delay. While

To further understand the model of Diévert et al. [15] over-predicts the first-stage ignition delay, we have conducted adiabatic, constant volume simulations (called CONV simulations), as these simulations are not linked to a particular

experiment by the volume trace and can be conducted over a wide range of temperatures. In the CONV simulations, overall ignition delay is defined as an increase in the temperature of 400 K over the initial temperature. The diluent for all of the CONV simulations is pure argon, although the RCM simulations described previously consider the diluent mixture associated with each experiment (either pure argon or a 50:50 mixture of argon and nitrogen by mole, see Table 1 and the Supplementary Material).

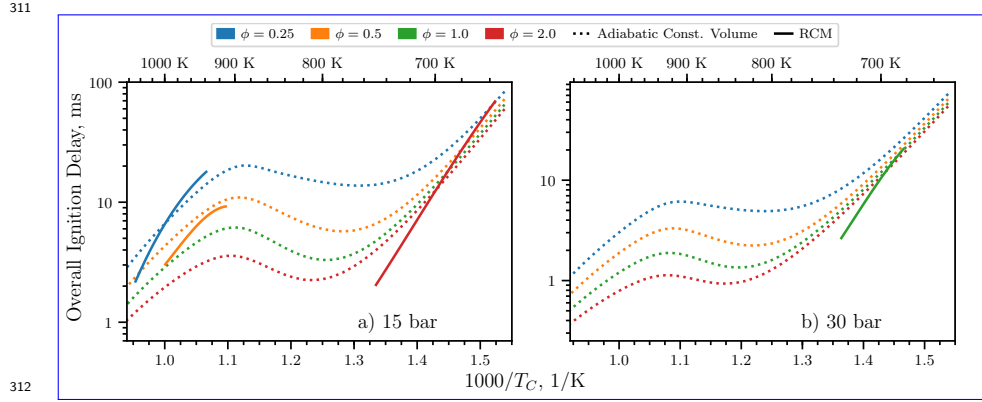


Figure 6: Comparison of simulated overall ignition delays computed in an adiabatic, constant volume system (dotted lines) and computed using the procedure described in Section 3.1 (solid lines). a) 15 bar, b) 30 bar.

Figure 6 compares the CONV simulations to the RCM simulations shown in Fig. 5. From Fig. 6, it can be seen that the curvature in the RCM simulations at  $P_C = 15$  bar,  $\phi = 0.25$  and  $0.5$  is related to the NTC region of the overall ignition delay, while the lack of curvature in the  $P_C = 15$  bar,  $\phi = 2.0$  and the  $P_C = 30$  bar,  $\phi = 1.0$  simulations is because those lie on the low-temperature side of the predicted NTC. It is clear from Fig. 6 that the model of Diévert et al. [15] predicts the NTC to occur at too high a temperature relative to the experiments.

To elucidate the underlying reasons for the disagreement between the Diévert et al. [15] model and the data, we constructed conduct simulations with an ad-



ditional model constructed using RMG (see Section 3.2). As can be seen in Fig. 5a, the agreement between the RMG model (dashed lines) and the experimental data is similar to the Diévert et al. [15] model for the ~~15-bar~~ $P_C = 15$  bar,  $\phi = 0.25$  and  $0.5$  data. Moreover, the RMG model predicts a similar NTC region as temperature is decreasing. For the ~~15-bar~~ $P_C = 15$  bar,  $\phi = 2.0$  data, the RMG model tends to over-predict the low-temperature ~~ignition delays, overall~~ignition delays (i.e., those to the right of the experimental NTC region on the Arrhenius plot), and does not predict the NTC region found experimentally. As before, the trend at ~~30-bar~~ $P_C = 30$  bar,  $\phi = 1.0$  is similar to the ~~15-bar~~ $P_C = 15$  bar,  $\phi = 2.0$  data; the RMG model over-predicts the low-temperature overall ignition delays and does not predict the experimental NTC region. Finally, as in the Diévert et al. [15] model, two-stage ignition is predicted for all of the  $\phi = 1.0$  and  $\phi = 2.0$  data shown in Fig. 5. However, the first-stage ignition delays are  $0.1$  ms to  $0.5$  ms less than the overall ignition delays, and are not shown on Fig. 5 because they are nearly indistinguishable from the overall ignition delay. ~~Again, the over-prediction of the first-stage ignition delay and pressure rise requires further investigation and understanding of the complex low-temperature chemistry.~~

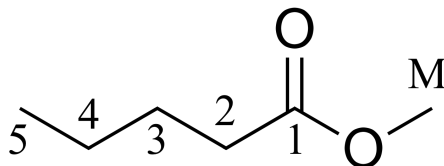
It is clear that neither model is able to predict the ignition delays of MV particularly well. In addition to the poor agreement shown in Fig. 5, the simulations for  $P_C = 15$  bar,  $\phi = 1.0$  and  $P_C = 30$  bar,  $\phi = 0.25, 0.5$  and  $2.0$  showed substantial heat release during the compression stroke (i.e., the simulations are much too reactive), and so these conditions ~~aren't~~are not compared in Fig. 5. We note again that the model by Diévert et al. [15] was validated for MV combustion only by comparison to flame extinction limits, so the disagreement is not wholly surprising.

In general, there could be three likely sources of error in the models: missing reaction pathways, incorrect values of the reaction rates, and incorrect values for thermodynamic properties of the species. We have noted in Section 3.2 that the RMG model has many more reactions than the Diévert et al. [15] model and the algorithm used in RMG considers a substantial number of the possible

pathways. This reduces the possibility of missing reaction pathways affecting the model. Further detailed studies are required to ensure that the RMG model includes all of the relevant reaction pathways, which are outside the scope of this work.

The second source of error may be incorrect reaction rate parameters, either because the rates are specified incorrectly in the model or because the rates are not well estimated by the typical analogy based-rules. It should be noted that errors of this type may affect the model generated by RMG—if the rates are not estimated correctly, reactions that are important in reality may not be included in the model. Determining the accuracy of the reaction rates used in the RMG and Diévar et al. [15] models requires further detailed studies of the models, which are also outside the scope of this work. Another, related, source of error could be incorrect estimation of the pressure dependence of the reaction rates, which may be particularly important for the isomerization reactions prevalent in low-temperature chemistry.

The third source of error may lie in the estimation of the thermodynamic properties of the species, particularly the fuel radicals. In the work of Diévar et al. [15], the program THERM~~[43]~~ is [43] was used to estimate thermodynamic values using the group additivity method. In the RMG model constructed in this work, RMG itself estimates the thermodynamic properties of the molecules also using the group additivity method. Nonetheless, the two models have differing predictions of the thermodynamic properties of the species in the model, particularly the fuel and its radicals. The values of the heats of formation of the fuel and its H-atom abstraction radicals are shown in Table 3; the radicals are labeled according to the convention shown in Fig. 7.



381

Figure 7: Structure of MV with carbon atoms labeled according to the convention used in

Table 3 and Table 4

Table 3 shows that the heats of formation of the fuel and radicals 3, 4, 5, and M are quite similar between the two mechanisms. However, the heat of formation of the second radical, the one closest to the methyl ester group, has a significantly lower heat of formation in the model by Diévert et al. [15] than in the RMG model. Note that it is expected that the second radical will be somewhat more stable than the other radicals, due to the influence of the methyl ester group on the adjacent carbon atom.

Table 3: Heats of formation of MV and its radicals, labeled according to the convention used in Fig. 7

Radical Site	Diévert et al. [15]		RMG Model (this work)	
	[kJ/mol]	[kcal/mol]	[kJ/mol]	[kcal/mol]
MV	-470.98	-112.57	-472.53	-112.94
2	-297.16	-71.02	-273.63	-65.40
3	-277.03	-66.21	-273.63	-65.40
4	-277.03	-66.21	-278.61	-66.59
5	-265.94	-63.56	-267.53	-63.94
M	-270.51	-64.65	-270.12	-64.56

~~Table 3 shows that the heats of formation of the fuel and radicals 3, 4, 5, and M are quite similar between the two mechanisms. However, the heat of formation of the second radical, the one closest to the methyl ester group, has a significantly lower heat of formation in the model by Diévert et al. [15] than in the RMG model. Note that it is expected that the second radical will be somewhat more stable than the other radicals, due to the influence of the methyl ester group on the adjacent carbon atom.~~

This difference in heats of formation affects the pathways that consume the fuel. By conducting a reaction pathway analysis to determine which radicals are formed from the breakdown of the fuel, we can analyze the proportion of each

radical formed as the fuel breaks down during the autoignition process. The following analysis is conducted for a constant volume, adiabatic simulation with initial temperature and pressure of 700 K, ~~30 bar, and 30 bar, respectively,~~ and for the stoichiometric equivalence ratio. The rates of production of the species have been integrated until the time of 20 % fuel consumption. The results of this analysis are shown in Table 4 for the two models. The percentages shown in ~~the~~ Table 4 are the percent of the fuel consumed to form a particular fuel radical by all the reactions that can form that radical, and the radicals are labeled according to the convention in Fig. 7.

~~Percent of MV consumed to form fuel radical species with a hydrogen atom missing at the location indicated in the first column and Fig. 7 Radical Site~~  
~~Diévar et al. [15] %RMG Model %RMG switched %2 29.2 12.5 11.0 3 17.5 12.2~~  
~~11.1 4 17.5 50.6 56.6 5 9.5 3.9 4.3 M 26.3 20.8 16.9~~

At the relatively low temperature and high pressure condition of this analysis, all of the fuel is consumed by H-atom abstractions to form the fuel radicals shown. It can be seen that the two models have quite different distributions of products from the first H-abstraction reactions. The model of ~~[15]~~ Diévar et al. [15] predicts that H-abstraction from the second carbon is the most prevalent, while the RMG model predicts that the radical on the fourth carbon in the chain will be primarily formed. This is in line with the heats of formation in Table 3, where the most stable radical (i.e., the radical with the smallest heat of formation) is most likely to be formed in each model.

Table 4: Percent of MV consumed to form fuel radical species with a hydrogen atom missing at the location indicated in the first column and Fig. 7

Radical Site	Diévert et al. [15] [%]	RMG Model [%]	RMG switched [%]
2	29.2	12.5	11.0
3	17.5	12.2	11.1
4	17.5	50.6	56.6
5	9.5	3.9	4.3
M	26.3	20.8	16.9

To further compare the models with each other, the NASA polynomials representing the thermodynamic properties of MV and the 5 fuel radicals from the model of Diévert et al. [15] ~~and~~ are used to replace the equivalent molecules in the RMG model. The results of a path analysis at the same condition as the other analysis is shown in Table 4 in the “RMG switched” column. ~~This analysis shows~~ The results of the analysis of the “RMG switched” model show that the radical on the fourth carbon ~~atom~~ is still the most ~~prevalant, despite changing~~ prevalent, despite the heats of formation ~~of the fuel and its radicals, for the fuel radicals in the “RMG switched” model being identical to the Diévert et al. [15] model.~~ This suggests that the reaction pathways have a substantial impact on the simulation, in addition to the influence of the thermochemistry, as discussed previously. Moreover, since the thermochemistry of the species in a reaction controls the reverse reaction rate of a reaction, the RMG algorithm may miss important pathways due to improperly estimated thermochemistry.

Taken together, these results show that the poor performance in a given model cannot be attributed to a single source. ~~There is a strong interaction between the thermodynamics of the species and the kinetics of the reactions, requiring~~ Separating the influence of thermochemistry and kinetics requires further detailed study of the methyl ~~ester system~~ valerate system specifically, and methyl ester systems more generally. Although such detailed work has begun, for example, with the work of Hayes and Burgess [14], further work is required to accurately predict the low temperature ignition delays of methyl valerate.

## 449 6. Conclusions

450 In this study, we have measured ignition delays for methyl valerate over a  
451 wide range of engine-relevant pressures, temperatures, and equivalence ratios.  
452 An NTC region of the [overall](#) ignition delay and two-stage ignition are recorded  
453 for pressures of 15 bar at  $\phi = 2.0$  and 30 bar at  $\phi = 1.0$ . A detailed chemical  
454 kinetic model available in the literature is unable to reproduce the experimental  
455 results, so a new model is constructed using the Reaction Mechanism Generator  
456 software. Although the new model contains many more reactions than the  
457 literature model, it is still unable to predict the experimental ignition delays  
458 satisfactorily. Both models predict an NTC region of the [overall](#) ignition delay  
459 under conditions where none is found in the experiments, and fail to predict  
460 the NTC region of [overall](#) ignition delay that is present in the experiments.  
461 Possible reasons for the discrepancy include missing reaction pathways, incorrect  
462 rate estimates, and incorrect thermodynamic property estimates. Comparative  
463 analysis of the two models failed to identify a single source of the error, and  
464 further detailed studies are required to improve predictions of the ignition delay  
465 at these engine-relevant conditions.

## 466 7. Acknowledgments

467 The authors acknowledge support from the Combustion Energy Frontier  
468 Research Center, an Energy Frontier Research Center funded by the U.S. De-  
469 partment of Energy, Office of Science, Office of Basic Energy Sciences, under  
470 award number DE-SC0001198.

## 471 References

- 472 [1] S. K. Hoekman, C. Robbins. Review of the effects of biodiesel  
473 on NOx emissions. Fuel Processing Technology 96 (2012) 237–249.  
474 doi:10.1016/j.fuproc.2011.12.036.

- 475 [2] J. Y. Lai, K. C. Lin, A. Violi. Biodiesel combustion: Advances in chemical  
476 kinetic modeling. *Progress in Energy and Combustion Science* 37 (2011)  
477 1–14. doi:10.1016/j.pecs.2010.03.001.
- 478 [3] L. Coniglio, H. Bennadji, P. Glaude, O. Herbinet, F. Billaud. Combustion  
479 chemical kinetics of biodiesel and related compounds (methyl and  
480 ethyl esters): Experiments and modeling – Advances and future refinements.  
481 *Progress in Energy and Combustion Science* 39 (2013) 340–382.  
482 doi:10.1016/j.pecs.2013.03.002.
- 483 [4] W. K. Metcalfe, S. Dooley, H. J. Curran, J. M. Simmie, A. M. El-Nahas,  
484 M. V. Navarro. Experimental and modeling study of C<sub>5</sub>H<sub>10</sub>O<sub>2</sub> ethyl and  
485 methyl esters. *The Journal of Physical Chemistry A* 111 (2007) 4001–4014.  
486 doi:10.1021/jp067582c.
- 487 [5] S. M. Walton, M. S. Wooldridge, C. K. Westbrook. An experimental  
488 investigation of structural effects on the auto-ignition properties of two  
489 C<sub>5</sub> esters. *Proceedings of the Combustion Institute* 32 (2009) 255–262.  
490 doi:10.1016/j.proci.2008.06.208.
- 491 [6] S. Dooley, H. J. Curran, J. M. Simmie. Autoignition mea-  
492 surements and a validated kinetic model for the biodiesel surro-  
493 gate, methyl butanoate. *Combustion and Flame* 153 (2008) 2–32.  
494 doi:10.1016/j.combustflame.2008.01.005.
- 495 [7] B. Akih-Kumgeh, J. M. Bergthorson. Comparative Study of Methyl Bu-  
496 tanoate and n -Heptane High Temperature Autoignition. *Energy & Fuels*  
497 24 (2010) 2439–2448. doi:10.1021/ef901489k.
- 498 [8] B. Akih-Kumgeh, J. M. Bergthorson. Structure-reactivity trends of C<sub>1</sub>–C<sub>4</sub>  
499 alkanolic acid methyl esters. *Combustion and Flame* 158 (2011) 1037–1048.  
500 doi:10.1016/j.combustflame.2010.10.021.
- 501 [9] K. Hadj-Ali, M. Crochet, G. Vanhove, M. Ribaucour, R. Minetti. A study

- of the low temperature autoignition of methyl esters. *Proceedings of the Combustion Institute* 32 (2009) 239–246. doi:10.1016/j.proci.2008.09.002.
- [10] K. Kumar, C.-J. Sung. Autoignition of methyl butanoate under engine relevant conditions. *Combustion and Flame* 171 (2016) 1–14. doi:10.1016/j.combustflame.2016.04.011.
- [11] E. Fisher, W. J. Pitz, H. J. Curran, C. K. Westbrook. Detailed chemical kinetic mechanisms for combustion of oxygenated fuels. *Proceedings of the Combustion Institute* 28 (2000) 1579–1586. doi:10.1016/S0082-0784(00)80555-X.
- [12] O. Korobeinichev, I. Gerasimov, D. Knyazkov, A. Shmakov, T. Bolshova, N. Hansen, C. K. Westbrook, G. Dayma, B. Yang. An Experimental and Kinetic Modeling Study of Premixed Laminar Flames of Methyl Pentanoate and Methyl Hexanoate. *Zeitschrift für Physikalische Chemie* 229 (2015). doi:10.1515/zpch-2014-0596.
- [13] A. M. Dmitriev, D. A. Knyazkov, T. A. Bolshova, A. G. Shmakov, O. P. Korobeinichev. The effect of methyl pentanoate addition on the structure of premixed fuel-rich n-heptane/toluene flame at atmospheric pressure. *Combustion and Flame* 162 (2015) 1964–1975. doi:10.1016/j.combustflame.2014.12.015.
- [14] C. Hayes, D. R. Burgess. Exploring the oxidative decompositions of methyl esters: Methyl butanoate and methyl pentanoate as model compounds for biodiesel. *Proceedings of the Combustion Institute* 32 (2009) 263–270. doi:10.1016/j.proci.2008.05.075.
- [15] P. Diévert, S. H. Won, J. Gong, S. Dooley, Y. Ju. A comparative study of the chemical kinetic characteristics of small methyl esters in diffusion flame extinction. *Proceedings of the Combustion Institute* 34 (2013) 821–829. doi:10.1016/j.proci.2012.06.180.



- [16] G. Mittal, C.-J. Sung. A Rapid Compression Machine for Chemical Kinetics Studies at Elevated Pressures and Temperatures. *Combustion Science and Technology* 179 (2007) 497–530. doi:10.1080/00102200600671898.
- [17] G. Mittal, C.-J. Sung. Aerodynamics inside a rapid compression machine. *Combustion and Flame* 145 (2006) 160–180. doi:10.1016/j.combustflame.2005.10.019.
- [18] B. W. Weber, C.-J. Sung. UConnRCMPy: Python-based Data Analysis for Rapid Compression Machines. in: S. Benthall, S. Rostrup (Eds.), *Proceedings of the 15th Python in Science Conference*, pp. 36–44. [http://conference.scipy.org/proceedings/scipy2016/bryan\\_weber.html](http://conference.scipy.org/proceedings/scipy2016/bryan_weber.html).
- [19] B. W. Weber, R. Fang, C.-J. Sung. UConnRCMPy, 2017. v3.0.5. doi:10.5281/zenodo.815569.
- [20] D. G. Goodwin, H. K. Moffat, R. L. Speth. Cantera: An Object-oriented Software Toolkit for Chemical Kinetics, Thermodynamics, and Transport Processes, 2017. v2.3.0. doi:10.5281/zenodo.170284.
- [21] S. van der Walt, S. C. Colbert, G. Varoquaux. The NumPy Array: A Structure for Efficient Numerical Computation. *Computing in Science & Engineering* 13 (2011) 22–30. doi:10.1109/MCSE.2011.37.
- [22] E. Jones, T. Oliphant, P. Peterson, et al. SciPy: Open source scientific tools for Python, 2001–. <https://scipy.org>.
- [23] J. D. Hunter. Matplotlib: A 2D Graphics Environment. *Computing in Science & Engineering* 9 (2007) 90–95. doi:10.1109/MCSE.2007.55.
- [24] D. Lee, S. Hochgreb. Rapid Compression Machines: Heat Transfer and Suppression of Corner Vortex. *Combustion and Flame* 114 (1998) 531–545. doi:10.1016/S0010-2180(97)00327-1.
- [25] B. W. Weber, K. Kumar, Y. Zhang, C.-J. Sung. Autoignition of n-butanol at elevated pressure and low-to-intermediate temperature 158 (???) 809–819. doi:10.1016/j.combustflame.2011.02.005.

- [26] K. Kumar, G. Mittal, C.-J. Sung. Autoignition of n-decane under elevated pressure and low-to-intermediate temperature conditions 156 (2009) 1278–1288. doi:10.1016/j.combustflame.2009.01.009.
- [27] A. K. Das, C.-J. Sung, Y. Zhang, G. Mittal. Ignition delay study of moist hydrogen/oxidizer mixtures using a rapid compression machine 37 (2012) 6901–6911. doi:10.1016/j.ijhydene.2012.01.111.
- [28] J. Ortega, F. Espiau, J. Tojo, J. Canosa, A. Rodríguez. Isobaric Vapor-Liquid Equilibria and Excess Properties for the Binary Systems of Methyl Esters + Heptane. *Journal of Chemical & Engineering Data* 48 (2003) 1183–1190. doi:10.1021/jc030117d.
- [29] A. G. Camacho, J. M. Moll, S. Canzonieri, M. A. Postigo. Vapor-Liquid Equilibrium Data for the Binary Methyl Esters (Butyrate, Pentanoate, and Hexanoate) (1) + Propanenitrile (2) Systems at 93.32 kPa. *Journal of Chemical & Engineering Data* 52 (2007) 871–875. doi:10.1021/jc060469v.
- [30] R. M. Stephenson, S. Malanowski, D. Ambrose, *Handbook of the Thermodynamics of Organic Compounds*, Elsevier, New York, 1987.
- [31] A. C. van Genderen, J. van Miltenburg, J. G. Blok, M. J. van Bommel, P. J. van Ekeren, G. J. van den Berg, H. A. Oonk. Liquid–vapour equilibria of the methyl esters of alkanolic acids: Vapour pressures as a function of temperature and standard thermodynamic function changes. *Fluid Phase Equilibria* 202 (2002) 109–120. doi:10.1016/S0378-3812(02)00097-3.
- [32] S. P. Verevkin, V. N. Emel’yanenko. Transpiration method: Vapor pressures and enthalpies of vaporization of some low-boiling esters. *Fluid Phase Equilibria* 266 (2008) 64–75. doi:10.1016/j.fluid.2008.02.001.
- [33] E. E. Dames, A. S. Rosen, B. W. Weber, C. W. Gao, C.-J. Sung, W. H. Green. A detailed combined experimental and theoretical study on dimethyl ether/propane blended oxidation. *Combustion and Flame* 168 (2016) 310–330. doi:10.1016/j.combustflame.2016.02.021.

- [34] A. C. Hindmarsh, P. N. Brown, K. E. Grant, S. L. Lee, R. Serban, D. E. Shumaker, C. S. Woodward. SUNDIALS: Suite of nonlinear and differential/algebraic equation solvers. *ACM Transactions on Mathematical Software* 31 (2005) 363–396. doi:10.1145/1089014.1089020.
- [35] S. C. Chapra, R. P. Canale, *Numerical Methods for Engineers*, McGraw-Hill Higher Education, Boston, 6th ed edition, 2010.
- [36] B. W. Weber, K. E. Niemeyer. ChemKED: A human- and machine-readable data standard for chemical kinetics experiments. Submitted to: *International Journal of Chemical Kinetics* (2017). [arXiv:1706.01987](#).
- [37] J. W. Allen, C. F. Goldsmith, W. H. Green. Automatic estimation of pressure-dependent rate coefficients. *Physical Chemistry Chemical Physics* 14 (2012) 1131–1155. doi:10.1039/c1cp22765c.
- [38] B. W. Weber, C.-J. Sung, M. W. Renfro. On the uncertainty of temperature estimation in a rapid compression machine. *Combustion and Flame* 162 (2015) 2518–2528. doi:10.1016/j.combustflame.2015.03.001.
- [39] G. Kukkadapu, K. Kumar, C.-J. Sung, M. Mehl, W. J. Pitz. Experimental and surrogate modeling study of gasoline ignition in a rapid compression machine. *Combustion and Flame* 159 (2012) 3066–3078. doi:10.1016/j.combustflame.2012.05.008.
- [40] M. Ribaucour, R. Minetti, L. R. Sochet. Autoignition of n-pentane and 1-pentene: Experimental data and kinetic modeling. *Symposium (International) on Combustion* 27 (1998) 345–351. doi:10.1016/S0082-0784(98)80422-0.
- [41] J. Bugler, K. P. Somers, E. J. Silke, H. J. Curran. Revisiting the Kinetics and Thermodynamics of the Low-Temperature Oxidation Pathways of Alkanes: A Case Study of the Three Pentane Isomers. *The Journal of Physical Chemistry A* 119 (2015) 7510–7527. doi:10.1021/acs.jpca.5b00837.

- 612 [42] K. A. Heufer, J. Bugler, H. J. Curran. A comparison of longer alkane  
613 and alcohol ignition including new experimental results for n-pentanol and  
614 n-hexanol. *Proceedings of the Combustion Institute* 34 (2013) 511–518.  
615 doi:10.1016/j.proci.2012.05.103.
- 616 [43] E. R. Ritter, J. W. Bozzelli. THERM: Thermodynamic property estimation  
617 for gas phase radicals and molecules. *International Journal of Chemical*  
618 *Kinetics* 23 (1991) 767–778. doi:10.1002/kin.550230903.